International Journal of Earth, Energy and Environmental Sciences
ISSN: 2517-942X
Vol:12, No:2, 2018

Shear Modulus Degradation of a Liquefiable Sand Deposit by Shaking Table Tests

Henry Munoz, Muhammad Mohsan, Takashi Kiyota

***Abstract*—**Strength and deformability characteristics of a liquefiable sand deposit including the development of earthquake-induced shear stress and shear strain as well as soil softening via the progressive degradation of shear modulus were studied via shaking table experiments. To do so, a model of a liquefiable sand deposit was constructed and densely instrumented where accelerations, pressures, and displacements at different locations were continuously monitored. Furthermore, the confinement effects on the strength and deformation characteristics of the liquefiable sand deposit due to an external surcharge by placing a heavy concrete slab (i.e. the model of an actual structural rigid pavement) on the ground surface were examined. The results indicate that as the number of seismic-loading cycles increases, the sand deposit softens progressively as large shear strains take place in different sand elements. Liquefaction state is reached after the combined effects of the progressive degradation of the initial shear modulus associated with the continuous decrease in the mean principal stress, and the buildup of the excess of pore pressure takes place in the sand deposit. Finally, the confinement effects given by a concrete slab placed on the surface of the sand deposit resulted in a favorable increasing in the initial shear modulus, an increase in the mean principal stress and a decrease in the softening rate (i.e. the decreasing rate in shear modulus) of the sand, thus making the onset of liquefaction to take place at a later stage. This is, only after the sand deposit having a concrete slab experienced a higher number of seismic loading cycles liquefaction took place, in contrast to an ordinary sand deposit having no concrete slab.

***Keywords*—**Liquefaction, shaking table, shear modulus degradation, earthquake.

I. Introduction

THE Great East Japan Earthquake on March 11, 2011 (Mw 9.0) caused extensive damages in north-eastern Japan. For instance, particularly from the geotechnical perspective, soil liquefaction induced ground deformations and subsidence was encountered in areas such as, for instance, the Tokyo Bay coastal area (Tokyo) and the Urayasu city (Chiba). Recent experiences on earthquake-induced liquefaction show that once soil liquefies, it is likely to liquefy again by a subsequent earthquake event, e.g. the 2011 Christchurch (Ms 6.3) and the 2011 Great East Japan (Ms 9.0) earthquakes [1]. This fact suggests that in order to predict the extent of damage due to future earthquakes, keeping data of historical liquefaction events is extremely important. In this respect, updating hazard maps for disaster prevention and damage reduction has become one of the major research works in Japan.

To construct liquefaction hazard maps, relevant input data including mainly the relations between a liquefaction index (PL) and pavement settlement as a result of ground deformation may be needed to produce a relevant factor of safety against liquefaction (FL). For instance, quantification of liquefaction via surface settlement by liquefaction over a wide area by aerial laser measurements [1] has been useful to create a liquefaction sinking hazard map for disaster prevention. In this view, a number of factors influential on the dynamic behavior of soils such as the dynamic load, the soil type, the rate of pore pressure buildup, the shear stress and shear strains development as well as the softening characteristics are crucial to the extent of the resulting ground deformation and so settlement of pavement. Therefore, in order to investigate the strength and deformability characteristics of a liquefiable sand deposit on the associated induced surface settlement (i.e. ground deformation, settlement of ground and structural pavement settlement combined), a series of shaking table experiments on deposit models were conducted in the present study. Strength and deformability characteristics of the sand deposit such as shear stress and shear strain development, shear modulus degradation and others were obtained by direct measurement and back-calculation to further construct an experimental-analytical framework for discussion.

II. Experimental Study

A. Shaking Table Tests

A shaking table apparatus at The Institute of Industrial Science, The University of Tokyo, was used to carry out the experimental works. The shaking table primarily is composed of a hydraulic pump, an actuator and an accelerometer to monitor the input acceleration. These components are accompanied by a data acquisition system that consists of a set of signal amplifiers, signal convertors, a control panel and a computer system to store the output data.

A rectangular prismatic steel box (80 cm-length × 47 cm-wide×50 cm-high) was fixed to the shaking table (Fig. 1). The front side of the box comprises a transparent-tempered glass window to observe the displacements and deformations of the model during the shaking table tests.

The models were designed assuming a scale-down factor in length (i.e., the ratio in length between a prototype structure and its model), λ, equal to 20. So that, in this case, it was assumed that the model of a sand deposit of 0.4 m depth simulates an ordinary full-scale deposit having of 8.0 m depth.

H. Munoz is with the Institute of Industrial Science of the University of Tokyo, Komaba, Meguro-ku, Tokyo, 153-8505 Japan (corresponding author, phone: 03-5452-6149; fax: 03-5452-6752; e-mail: hmunoz@iis.u-tokyo.ac.jp).
M. Mohsan and T. Kiyota are with the Institute of Industrial Science of the University of Tokyo, Komaba, Meguro-ku, Tokyo, 153-8505 Japan (e-mail: mohsan@iis.u-tokyo.ac.jp, kiyota@iis.u-tokyo.ac.jp).

B. Sand Deposit Models

Two different sand-deposit models were constructed inside the steel box (Figs. 1 (a) and (b)): 1) Case 1: an ordinary sand deposit and 2) Case 2: an ordinary sand deposit with a concrete slab placed on its top. The concrete slab of 0.45 cm-length, 0.3 m-wide and 0.06 m-thickness (with 21 kN/m^3 for the concrete density) simulates a section of an actual concrete pavement on the ground surface.

The supporting ground layers in the deposits were produced by pluviating air-dried silica sand No. 5 (maximum density of 15.5 kN/m^3, minimum density of 12.7 kN/m^3, dry density of 14.0 kN/m^3, saturated density of 18.4 kN/m^3; specific gravity of 2.6) to obtain a relative density Dr of about 50%. To observe the deformation of the backfill during the shaking tests, thin horizontal layers (with a width of about 1 cm) of dyed silica sand were placed at a vertical spacing of 0.05 m immediately behind the front transparent glass window of the sand box (Fig. 1 (c)). The models were densely instrumented at locations relevant to monitor displacements, pore-water pressures and accelerations (see A, A1-6 and PWP1-2 in Fig. 1).

C. Dynamic Loading Method

Each model was subjected to sinusoidal base acceleration motion at a frequency of 10 Hz. The base acceleration amplitude was kept constant at about 300 gal (when a steady-state of the acceleration amplitude was reached), see Fig. 2. A frequency of 10 Hz was selected to be far below the initial natural frequency of the sand-deposit models under undamaged conditions.

The scale factor for frequency depends on the shear strain level expected to take place and cause damage by shear strain development in the granular material (i.e. silica sand).

For the considered scale factor for length, 1/λ= 1/20, the scale factor for frequency becomes about 4.5 [2], [3] for those relatively large values of shear strain in the order of 1%. Thus, considering the silica sand deposit in full scale to be shaken at typical predominant frequencies of strong earthquake motions (i.e. 1-3 Hz measured by the 1995 Hyogoken-Nambu earthquake), the input frequency in the model yields between 4.5 to 13.5 Hz (i.e. 4.5 times 1-3 Hz). Therefore, a frequency of 10 Hz, lower than the deposits natural frequencies, suffices to simulate relatively large shear-strain levels in the sand.

III. Evaluation of Shear Stress-Strain Induced by Shaking

Shear stress and strain histories at different points (i.e. A2, A3 in Figs. 1 (a), (b)) inside the sandy backfill were back-calculated from their respective set of acceleration record.

The characteristics of soil response during earthquake excitations in the field can be obtained evaluating the shear stress-strain histories form free-field down-hole accelerations [4]-[6]. This technique uses the one-dimensional shear beam idealization to describe the site seismic lateral response as:

$$\frac{\partial \tau}{\partial z} = \rho \ddot{u} \tag{1}$$

With boundary conditions $u\,(h,t) = \bar{u}$ and $\tau(0,t) = 0$. where t is the time; z is the depth coordinate; $\tau = \tau(z,t)$ is the horizontal shear stress; $\ddot{u} = \ddot{u}(z,t)$ is the absolute horizontal acceleration; $u = u(z,t)$ is the absolute displacement; $\bar{u} = \bar{u}(t)$ is the input or bedrock horizontal displacement; ρ is the assumed mass density; and h is the site depth. By integrating this equation of motion and using the stress-free surface boundary condition, the shear stress at any level z may be expressed as:

$$\tau(z,t) = \int_0^z \rho \ddot{u}\ dz \tag{2}$$

$$\tau_i(t) = \sum_{k=1}^{i-1} \rho \frac{\ddot{u}_k + \ddot{u}_{k+1}}{2} \Delta z_k\ , i = 2,3,\ldots, \tag{3}$$

where subscript i refers to level z_i; $\tau_i = \tau(z_i,t)$; $\ddot{u}_i = \ddot{u}(z_i,t)$; and Δz_k is the soil slice thickness.

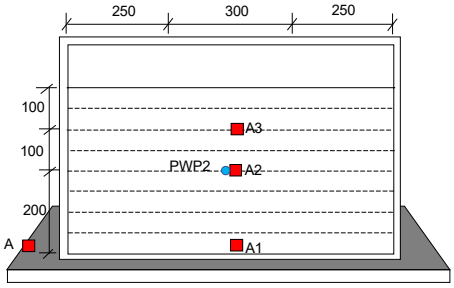

(a)

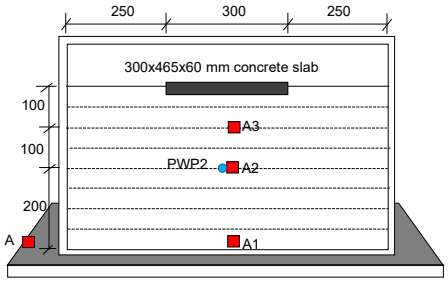

(b)

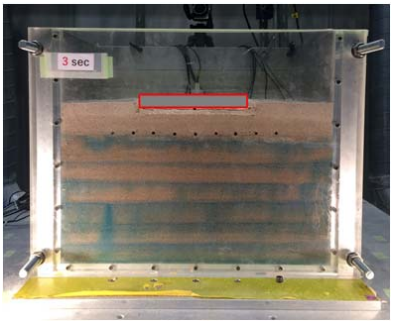

(c)

Fig. 1 Shaking table set up and instrumentation: (a) Case 1: a sand deposit with no concrete slab and (b) Case 2: a sand deposit with a concrete slab on its top (units: mm). A, A1-3 are accelerometers, PWP2 is pore pressure gauge. (c) Deposit after shaking

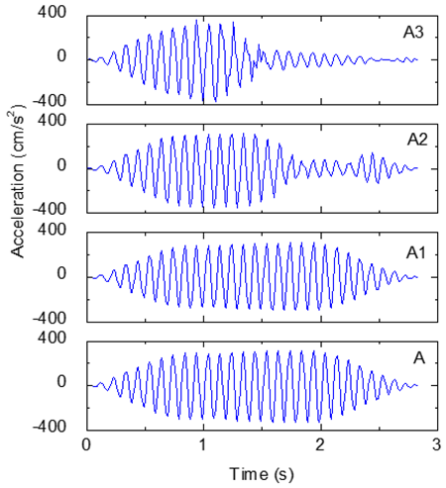

(a)

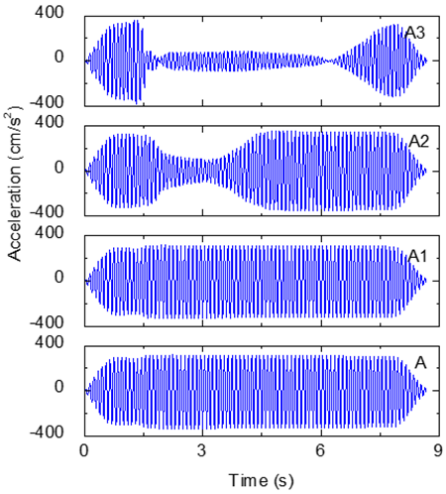

(b)

Fig. 2 Time history of acceleration for (a) Case 1 and (b) Case 2

The corresponding shear strain value, $\gamma_i(t)$, can be back-calculated using the displacement values obtained from the double integration of the acceleration-time histories as:

$$\gamma_i(t) = \frac{1}{\Delta z_{i-1} - \Delta z_i}\left[(u_{i+1} - u_i)\frac{\Delta z_{i-1}}{\Delta z_i} + (u_i - u_{i-1})\frac{\Delta z_i}{\Delta z_{i-1}}\right] \quad (4)$$

where $u_i = u(z_i, t)$ is the absolute displacement at the level z_i.

The equations proposed by [4]-[6] for field measurement utilize the acceleration recorded at surface as they deal with the site data. In laboratory tests, a reliable surface acceleration is rarely available as accelerometers need to be embedded in soil to maintained good contact. Therefore, the values of surface acceleration obtained by extrapolation with a linear fitting is recommended to be used [7] by the following approximation:

$$\ddot{u}(z = 0) = \ddot{u}_1 = \ddot{u}_2 + \frac{\ddot{u}_3 - \ddot{u}_2}{\Delta z_2}(-\Delta z_1) \quad (5)$$

IV. Test Results and Discussion

A. Shear Stress and Strain Development

Shear stress and strain histories of representative points inside the sand deposit when it is subjected to base shaking were analyzed. For this purpose, the records of the accelerations at locations A and A1-3 were used.

The total horizontal displacement of each of these accelerometers was back-calculated from its respective acceleration record by a double integration method. The acceleration records were firstly linear-baseline corrected and then filtered using a fourth-order Butterworth filtering procedure with a band-pass at 3 Hz to 25 Hz. The filtering procedure conducted thoroughly for the whole acceleration records did not change the nature of the actual measurements in the tests.

The estimated shear stress and shear strain histories for the representative points A2-3 at different stages of loading for Case 1 and Case 2 are depicted in Figs. 3 and 4, respectively.

By the above procedure, particularly very small amounts of shear stress and shear strain (i.e. shear strains in the order of 0.0001 to less than 0.01%) produced in the backfill at lower accelerations, i.e. at the firsts loading cycles, were difficult to obtain accurately. On the other hand, at relatively large shear strains (i.e. > 0.01%) encountered after the sand deposit was subjected to higher base accelerations, the estimated shear stress-strain quantities were accurately back-calculated.

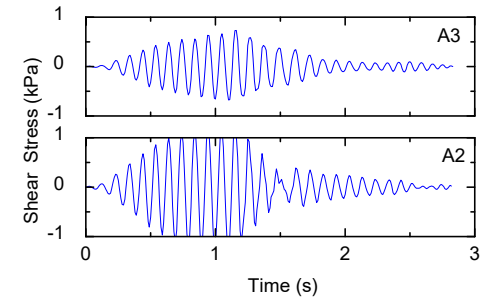

(a)

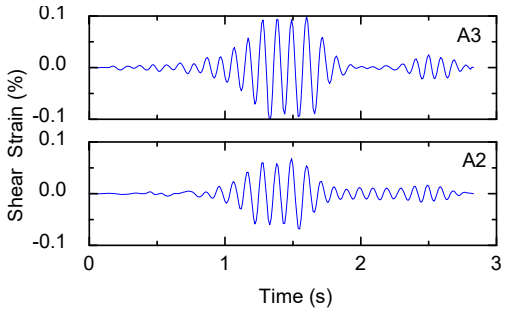

(b)

Fig. 3 Time history of (a) shear stress and (b) shear strain at locations A2 and A3 for Case 1

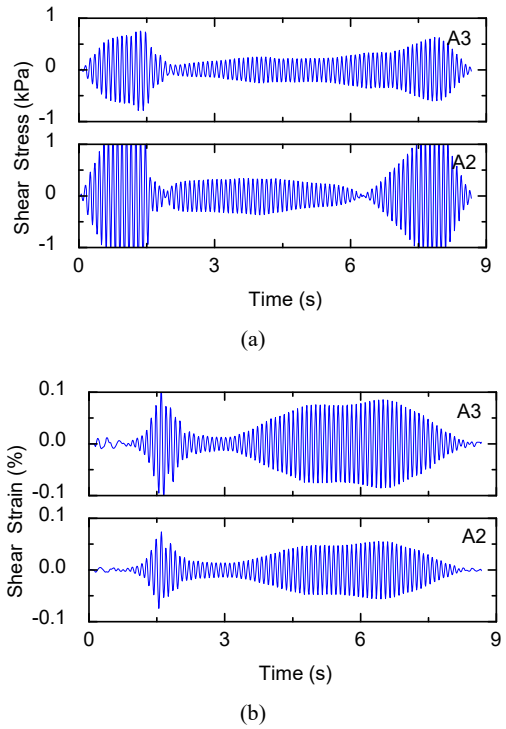

Fig. 4 Time history of (a) shear stress and (b) shear strain at locations A2 and A3 for Case 2

B. Shear Modulus Degradation

The shear moduli of the soil elements analyzed placed at A2, 3 in the backfill were calculated from the shear stress-strain loop developed cycle by cycle during the seismic load. See the shear stress-strain history in Fig. 5.

Phase difference and acceleration amplification (or de-amplification) at A2, 3 in contrast to the input acceleration at A, ultimately featured the characteristics of shear stress-shear strain loop associated with material shear modulus and energy dissipation (i.e. material damping and radiation damping by wave propagation) cycle by cycle throughout the tests [2].

The equivalent shear modulus, G during a shear stress-strain cycle is calculated by

$$G = \frac{\tau(\gamma_m)}{\gamma_m} \quad (6)$$

where γ_m is the maximum shear strain amplitude (single amplitude), and $\tau(\gamma_m)$ is the shear stress associated with γ_m for an equivalent linear system of stiffness G.

In general, the soil shear modulus back-calculated from the shaking table tests was found to decrease progressively in each loading cycle. This behavior can be attributed due to the following, although not limited to: 1) an increase in the shear strain amplitude at each loading cycle as shown in Fig. 5, 2) the buildup of pore pressure (u) as shown in Fig. 6 (only Case 1 is shown herein), and 3) the decrease of the initial mean principal stress p (i.e. $p = (\sigma_1 + \sigma_2 + \sigma_3)/3$ where σ_1, $\sigma_2 = \sigma_3$ are principal stresses at A1-6) before shaking (i.e. static condition) as a result of factor 2 (i.e. $p - u$). The latter agrees with previous findings in the literature which show that the shear modulus, for the same shear strain level, generally increases with a decrease in p [8] or other way, shear modulus decreases with p decreasing (i.e. the shear modulus dependency on shear strain level-p-void ratio).

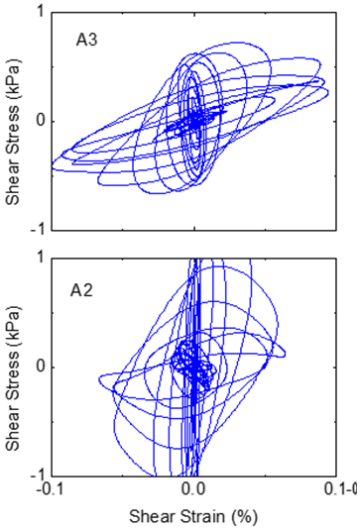

Fig. 5 Hysteretic shear stress-strain loops at locations A2 and A3 for Case 1

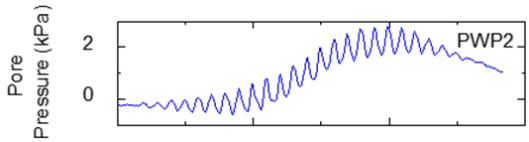

Fig. 6 Time history of pore pressure build up at location A2 for Case 1

Fig. 7 shows the shear modulus values back-calculated from the shaking table tests for Case 1 and Case 2 (numbers 0, 4, ,5, 10, 20, etc. represent the respective number of accumulated loading cycles).

In Fig. 7, in addition to the shear modulus results found out from the shaking table experiments (see open circles), shear modulus degradation curves have been plotted (see the continuous curves) using the formulations proposed by [8], [9].

For Case 1, under static conditions, the points A3 located at a 10-cm depth and A2 located to 20 cm below the ground surface are being subjected to p equal to 1.35 kPa-2.70 kPa (for $\sigma_3 = Ko\sigma_1$ where Ko=0.6 and backfill density of 18.4 kN/m^3). For Case 2, before the shaking event, in addition to the geostatic stresses (i.e. σ_1, $\sigma_2 = \sigma_3$), stresses at A2-3 take into account stresses induced by the weight of the concrete slab (i.e. the Westergaard stress distribution). Then, points at A2-3 are subjected to p about 1.35 kPa-2.70 kPa (degradation curves G-p in Fig. 7 with respective label of p shows this condition). Immediately after the beginning of shaking, p starts decreasing continuously towards p~0 at the onset of liquefaction as the pore pressure u increases. Degradation

curves for particular loading stages where p= 0.13 kPa-0.20 kPa are also shown in Fig. 7. Then, G values from the shaking table experiments in Fig. 7 are expected to move along their correspondent G-p degradation curve from their initial higher p.

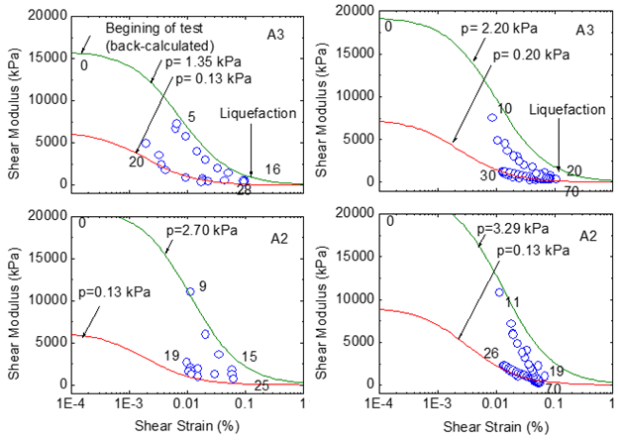

Fig. 7 Material stiffness back-calculated from the shaking table tests at locations A2 and A3 for (a) Case 1 and (b) for Case 2 (numbers 0, 10, 20, etc. represent respective loading cycles)

C. Softening and Liquefaction of the Sand Deposits

The dynamic performances of the sand deposits for Case 1 and Case 2 were compared herein. In this regard, and a number of advantages of having Case 2 came to light in contrast to Case 1 on the overall strength, deformability and softening characteristics of the liquefiable sand deposit.

In this instance, Fig. 8 shows the relationships between G-number of loading cycles for Case 1 and 2. The following main advantageous characteristics of having Case 2 over Case 1 can be cited, although not limited to:

1) Strength capacity: the initial stiffness (initial values of G) for Case 1 is slightly lower than for Case 2. This result indicates that by placing a slab on the top of the sand deposit, the confinement in the foundation soil is increased leading to an increase in the initial p and therefore an increase in the initial G (i.e. G_{max}), i.e. a higher material stiffness and a higher strength capacity of the deposit before a shaking event. Therefore, the result indicates that Case 2 may become more stable by high initial strength against seismic loads.
2) Softening rate: by analyzing Case 1 and 2, it can be observed that the initial stiffness inherent to each sand deposit decreases continuously at different rates towards their lowest G (i.e. G_{min}) during a pre-failure process (or pre-liquefaction state). That is, the initial stiffness of the sand deposit decreases firstly gradually and then faster with the increase in the number of seismic loading cycles. For instance, for Case 1 the G_{min} was reached relatively fast, i.e. G_{min} took place after a small number cycles (at 15-16 cycles) in contrast to Case 2 (19-20 cycles). This fact indicates that by placing a slab on the top of the sand deposit, the degradation of the initial shear modulus took place slowly and progressively and only after the deposit experienced higher loading cycles, G approached to G_{min}. This indicates that the deposit may experience shear failure in a more ductile fashion.

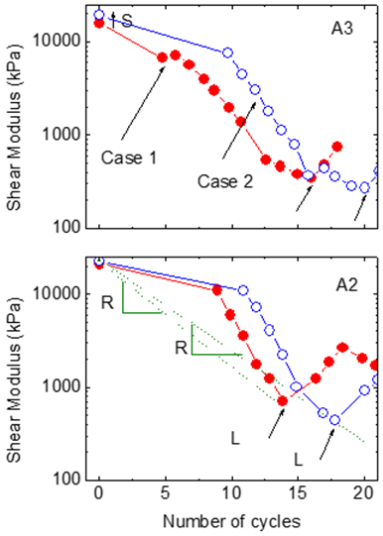

Fig. 8 History of material stiffness softening and the increasing number of loading cycles at locations A2 and A3 for Case 1 and Case 2. Letters S, R and L stand for strength capacity, softening rate and liquefaction state, respectively

3) Liquefaction state: The results indicate that by placing a slab on the top of the sand deposit, liquefaction can take place at a later state only after the deposit experience a higher number of loading cycles. This behavior may be the result of the combined effects of a) strength capacity, b) softening rate and c) pore pressure buildup (associated with decreasing p towards zero) on the sand deposit.

By analyzing Case 1 and 2, it was found that their respective liquefaction states (i.e. p~0) together with their lowest G (i.e. G_{min}) were reached at different rates and different number of loading cycles they were subjected to. That is, for Case 1, the combination of p~0 and G_{min} was reached after 15-16 cycles in contrast to the 19-20 cycles required for Case 2 to reach its liquefaction state.

In summary, among the two cases analyzed, Case 2 seems to be a more dynamically stable structure having a higher initial stiffness, a lower decreasing rate of stiffness making the deposit slightly more difficult to reach liquefaction.

V. Conclusion

From the above discussion, the initial observations can be reported. By increasing the surcharge on the top of a liquefiable sand deposit (i.e. by placing a concrete slab), it may become an effective measure to maintain the deposit dynamically more stable where liquefaction state may be reached at a later state. The following resulting new beneficial characteristics of the sand deposit include: 1) a higher strength capacity by having a higher initial stiffness, 2) a lower

softening rate of the initial stiffness and 3) the late onset of the liquefaction state.

ACKNOWLEDGMENT

H. Munoz is grateful to the Japan Society for the Promotion of Science (JSPS) for being supported through the JSPS Fellowship Program to conduct research activities.

REFERENCES

[1] Konagai, K. Kiyota, T. Suyama, S, Asakura, T., Shibuya T., Eto "Maps of soil subsidence for Tokyo bay shore areas liquefied in the March 11th, 2011 off the Pacific Coast of Tohoku Earthquake" Soil Dynamics and Earthquake Engineering, 53 (1):240-253, 2013.

[2] H. Munoz, F. Tatsuoka, D. Hirakawa, H. Nishikiori, R. Soma, M. Tateyama, K. Watanabe "Dynamic stability of geosynthetic-reinforced soil integral bridge" Geosynthtetics International, 19 (1) 11-38, 2012.

[3] F. Tatsuoka, H. Munoz, T. Kuroda, H. Nishikiori, R. Soma, T. Kiyota, M. Tateyama, K. Watanabe "Stability of existing bridges improved by structural integration and nailing" Soils and Foundations, 52 (3) (2012), pp. 430-448.

[4] Zeghal, M. and Elgamal, A-W. "Analysis of site liquefaction using earthquake records". Journal of Geotechnical Engineering, ASCE, 120, (6): 996-1017, 1994.

[5] Zeghal, M., Elgamal, A-W., and Tang, H. T. "Lotung downhole array. I: Evaluation of site dynamic properties: evaluation of soil nonlinear properties". Journal of Geotechnical Engineering, ASCE, 121 (4): 350-362, 1995.

[6] Zeghal, M., Elgamal, A-W., and Tang, H. T. "Lotung downhole array. II: Evaluation of soil nonlinear properties". Journal of Geotechnical Engineering, ASCE, 121 (4): 363-378, 1995.

[7] Brennan, A. J., Thusynthan, N. I. and Madabhushi, P. G "Evaluation of shear modulus and damping in dynamic centrifuge tests". Journal of Geotechnical and Geoenvironmental Engineering, ASCE, 131 (12): 1488-1497, 2005.

[8] Tatsuoka, F., Iwasaki, T. and Takagi Y. "Hysteretic damping of sands under cyclic loading and its relation to shear modulus". Soils and Foundations, 18 (2): 25-40, 1978.

[9] Shibata, T and Solearno, D. S. "Stress-strain characteristics of sand under cyclic loading". Proc. Japanese Society Civil Engineers, 239 (1): 57-75, 1976.